Supporting Information for

Screening Transition Metal Electrodes for Achieving near 100% Selectivity to Urea via Electroreduction of NO_3^- and CO_2 at 100 mA/cm^2 Current Density

Nishithan C. Kani[a#], Ishita Goyal[a#], Samuel Olusegun[b], Sreenivasulu Chinnabattigalla[c], Rajan R. Bhawnani[a], Ksenija D. Glusac[c, d], Joseph A. Gauthier[b]*, and Meenesh R. Singh[a]*

[a] Department of Chemical Engineering, University of Illinois Chicago, Chicago, IL 60607, United States.

[b] Department of Chemical Engineering, Texas Tech University, Lubbock, TX 79409, United States

[c] Department of Chemistry, University of Illinois Chicago, Chicago, IL 60607, United States

[d]Chemical Sciences and Engineering Division, Argonne National Laboratory, Lemont, Illinois 60439, United States.

[#] Authors contributed equally

* Corresponding Authors

***Corresponding Authors:**

Prof. Meenesh R. Singh, Email: mrsingh@uic.edu

Prof. Joseph A. Gauthier, Email: Joe.Gauthier@ttu.edu

Keywords: Electrochemical urea synthesis, Electrochemical nitrate reduction, Electrochemical CO_2 reduction, Nitrate removal, Electrochemical C-N coupling.

Table S1: Literature comparison of the urea FE and yield/current density.

Sr.No.	Catalyst	Reactants	Electrolyte	Urea FE	Urea Yield/Current Density	Reference
1	$BiFeO_3/BiVO_4$	N_2/CO_2	0.1 M $KHCO_3$	17.18 % at -0.4 V vs. RHE	-0.24 mA/cm^2 at -0.4 V vs. RHE	[1]
2	Bi-$BiVO_4$	N_2/CO_2	0.1 M $KHCO_3$	12.55 % at -0.4 V vs. RHE	-0.29 mA/cm^2 at -0.4 V vs. RHE	[2]
3	Te-Pd NCs	NO_2^-/CO_2	0.1 M $KHCO_3$/0.05 M KNO_2	12.2 % at -1.1 V vs. RHE	~-0.976 mA/cm^2 at -1.1 V vs. RHE	[3]
4	Ni phthalocyanine/GDE	NO_2^-/CO_2	0.2 M $KHCO_3$/0.02 M KNO_2	40 % at -1.5 V vs. SHE	-26 mA/cm2 at -1.5 V vs. SHE	[4]
5	Single atom Cu	NO_3^-/CO_2	0.1 M $KHCO_3$/0.1 M KNO_3	28 % at -0.9 V vs. RHE	-27 mA/cm^2 at -0.9 V vs. RHE	[5]
6	Ag-GDE	NO_2^-/CO_2	0.2 M $KHCO_3$/0.02 M KNO_2	38% at -1 V vs. SHE	~-3 mA/cm2 at -1 V vs. SHE	[6]
7	Indium oxyhydroxide	NO_3^-/CO_2	0.1 M KNO_3	51 % at -0.5 V vs. RHE	-0.43 mA/cm^2 at -0.5 V vs. RHE	[7]
8	Indium hydroxide	NO_3^-/CO_2	0.1 M KNO_3	53.4 % at -0.6 V vs. RHE	-0.36 mA/cm^2 at -0.6 V vs. RHE	[8]
9	Zn/GDE	NO_3^-/CO_2	0.2 M $KHCO_3$/0.02 M KNO_3	35 % at -1.75 V vs. RHE	NR	[9]
10	ZnO porous nano sheets	NO_2^-/CO_2	0.2 M $NaHCO_3$/0.1 M $NaNO_2$	23.26 % at -0.79 V vs. RHE	-27 mA/cm^2 at -0.79 V vs. RHE	[10]
11	PdCu nanoalloy loaded on TiO_2	N_2/CO_2	NR	8.92% at -0.4 V vs. RHE	3.36 mmol g^{-1} h^{-1} at −0.4 V vs. RHE	[11]
12	ZnO Nanosheets	NO/CO2	0.2 M KHCO3	11.26% at -0.92V vs. RHE	-40 mA/ cm^{-2} at -0.92V vs. RHE	[12]

13	PdCu nanoalloy loaded on TiO2	N2/CO2	0.1M KHCO3	8.92% at -0.4 V vs. RHE	-0.11 mA/cm^2 at -0.4 V vs. RHE	[13]
14	Diatomic Fe-Ni	NO_3^-/CO_2	0.1 M $KHCO_3$ with 50 Mm KNO_3	17.8% at -1.5V vs. RHE	-1.73 mA/cm^2 at -1.5 V vs. RHE	[14]
15	Titania–Nafion Composite	CO_2 /NO_3^-	CO2-saturated 0.1m KNO3	40 % at -0.98 V vs Ag/AgCl	-0.18 mA/cm^2 at -0.98 V vs Ag/AgCl	[15]
16	copper phthalocyanine nanotubes	N_2 /CO_2	0.1 M $KHCO_3$	12.99% at –0.6 V vs RHE	143.47 μg h^{-1} mg^{-1}	[16]

Table S2: Details of the chemicals used for the current study.

Sr No.	Chemicals	Purity (%)	Catalog Number	Manufacturer
1	Potassium Bicarbonate	99.7	237205	Sigma Aldrich
2	Potassium Nitrate	99.0	221295	Sigma Aldrich
3	Thiosemicarbazide	99	T33405	Sigma Aldrich
4	2, 3 - Butanedione Monoxime	98	B0753	Sigma Aldrich
5	Phenol Nitroprusside solution	NA	P6994	Sigma Aldrich
6	Sodium Hypochlorite solution	NA	239305	Sigma Aldrich
7	Sulfuric Acid	95.0 - 98.0	258105	Sigma Aldrich
8	Phosphoric Acid	85	BDH3118	BDH
9	Nitric Acid	25	1.60317	Sigma Aldrich
10	Iron (III) Chloride	97	157740	Sigma Aldrich
11	Potassium Hydroxide	99.99	306568	Sigma Aldrich
12	Urea	99.5	17131901	Cytiva (GEH Life Sciences)
13	Ammonia Solution	25	105428	Sigma Aldrich

14	Carbon Dioxide gas	99.999	UN1013	Linde
15	Argon Gas	99.999	UN1006	Linde

Table S3: Details of the materials used for the current study.

Sr No.	**Materials**	**Purity (%)**	**Catalog Number**	**Manufacturer**
1	Silver Electrode	99.999	NA	ACI Alloys
2	Platinum Electrode	99.999	NA	ACI Alloys
3	Silver-Silver Chloride Reference Electrode	NA	NA	Innovative Instruments
4	Rigid Resin 10K	NA	FLRG1001	Formlabs
5	Nafion Membrane	NA	274674	Sigma
6	Iron Electrode	99.999	NA	ACI Alloys
7	Cobalt Electrode	99.999	NA	ACI Alloys
8	Nickel Electrode	99.999	NA	ACI Alloys
9	Copper Electrode	99.999	NA	ACI Alloys
10	Zinc Electrode	99.999	NA	ACI Alloys
11	Ruthenium Electrode	99.999	NA	ACI Alloys
12	Palladium Electrode	99.999	NA	ACI Alloys
13	Tungsten Electrode	99.999	NA	ACI Alloys
14	Rhenium Electrode	99.999	NA	ACI Alloys
15	Iridium Electrode	99.999	NA	ACI Alloys
16	Platinum Electrode	99.999	NA	ACI Alloys
17	Gold Electrode	99.999	NA	ACI Alloys
18	Indium Electrode	99.999	NA	ACI Alloys

19	Tin Electrode	99.999	NA	ACI Alloys
20	Lead Electrode	99.999	NA	ACI Alloys
21	Cobalt Sputtering Target	99.999	91017-CO	Electron Microscopy Sciences
22	Silver Sputtering Target	99.999	91017-AG	Electron Microscopy Sciences
23	Zinc Sputtering Target	99.999	91017-ZINC	Electron Microscopy Sciences
24	Copper Sputtering Target	99.999	91017-CU	Electron Microscopy Sciences
25	Carbon Substrate	NA	4655-T060	Fuel Cell Store

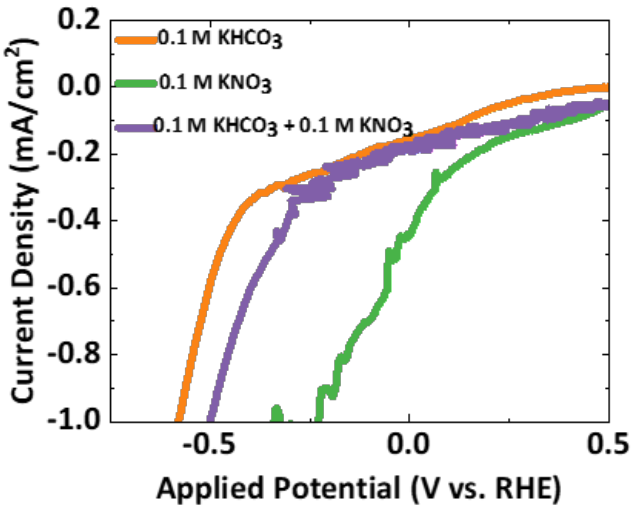

Figure S1: Linear sweep voltammetry (LSV) profiles for Ag cathode using different catholytes such as 0.1 M $KHCO_3$ (equilibrated with CO_2), 0.1 M KNO_3 and a solution of 0.1 M $KHCO_3$ and 0.1 M KNO_3 (equilibrated with CO_2).

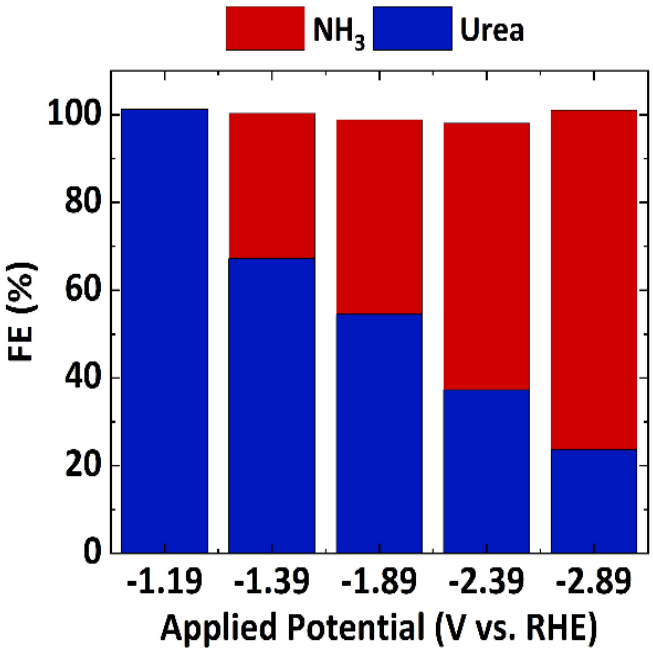

Figure S2: NH_3 and Urea FE at high over potentials.

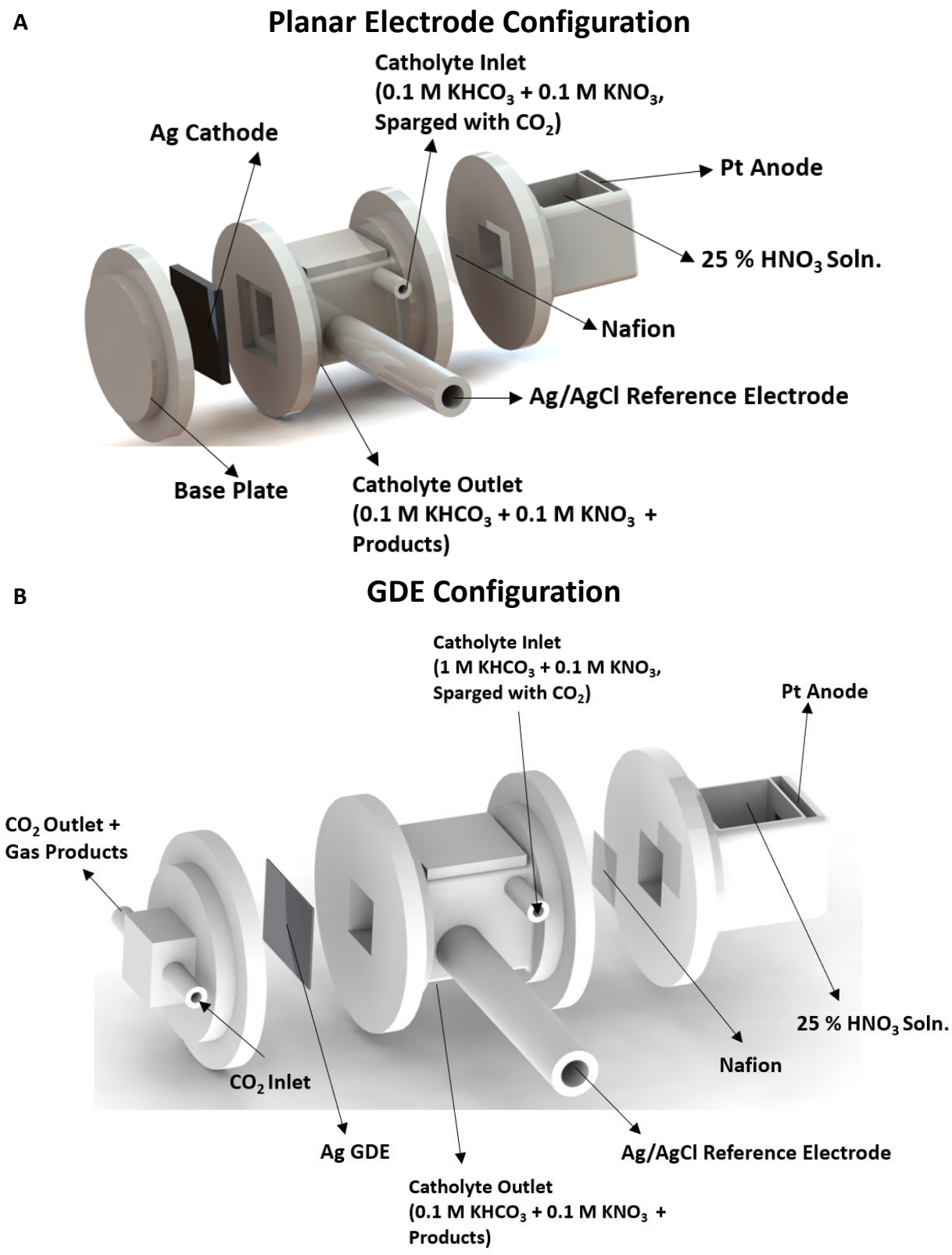

Figure S3: Reactor Schematic A) Planar Electrode Configuration. B) GDE Configuration.

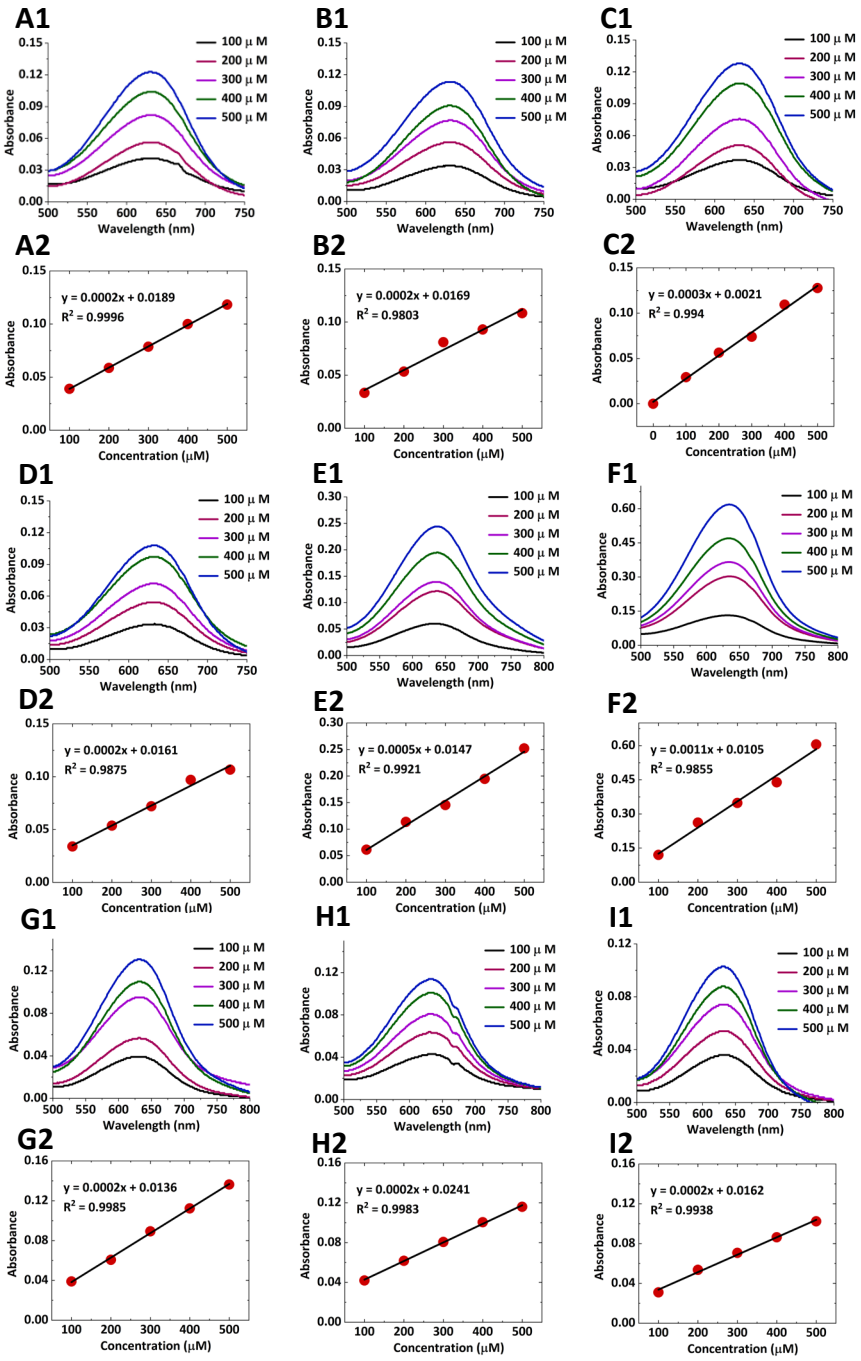

Figure S4: NH_3 calibration graphs Absorbance scans as a function of wavelengths. Absorbances as a function of NH_3 concentrations at 632 nm. Different concentrations of NH_3 are prepared in **A1, A2)** 1 M KNO_3 + 0.1 M $KHCO_3$ **B1, B2)** 0.5 M KNO_3 + 0.1 M $KHCO_3$ **C1, C2)** 0.1 M KNO_3 + 0.1 M $KHCO_3$ **D1, D2)** 0.01 M KNO_3 + 0.1 M $KHCO_3$ **E1, E2)** 0.001 M KNO_3 + 0.1 M $KHCO_3$ **F1, F2)** 0.1 M KNO_3 + 1 M $KHCO_3$ **G1, G2)** 0.1 M KNO_3 + 0.5 M $KHCO_3$ **H1, H2)** 0.1 M KNO_3 + 0.01 M $KHCO_3$ **I1, I2)** 0.1 M KNO_3 + 0.001 M $KHCO_3$.

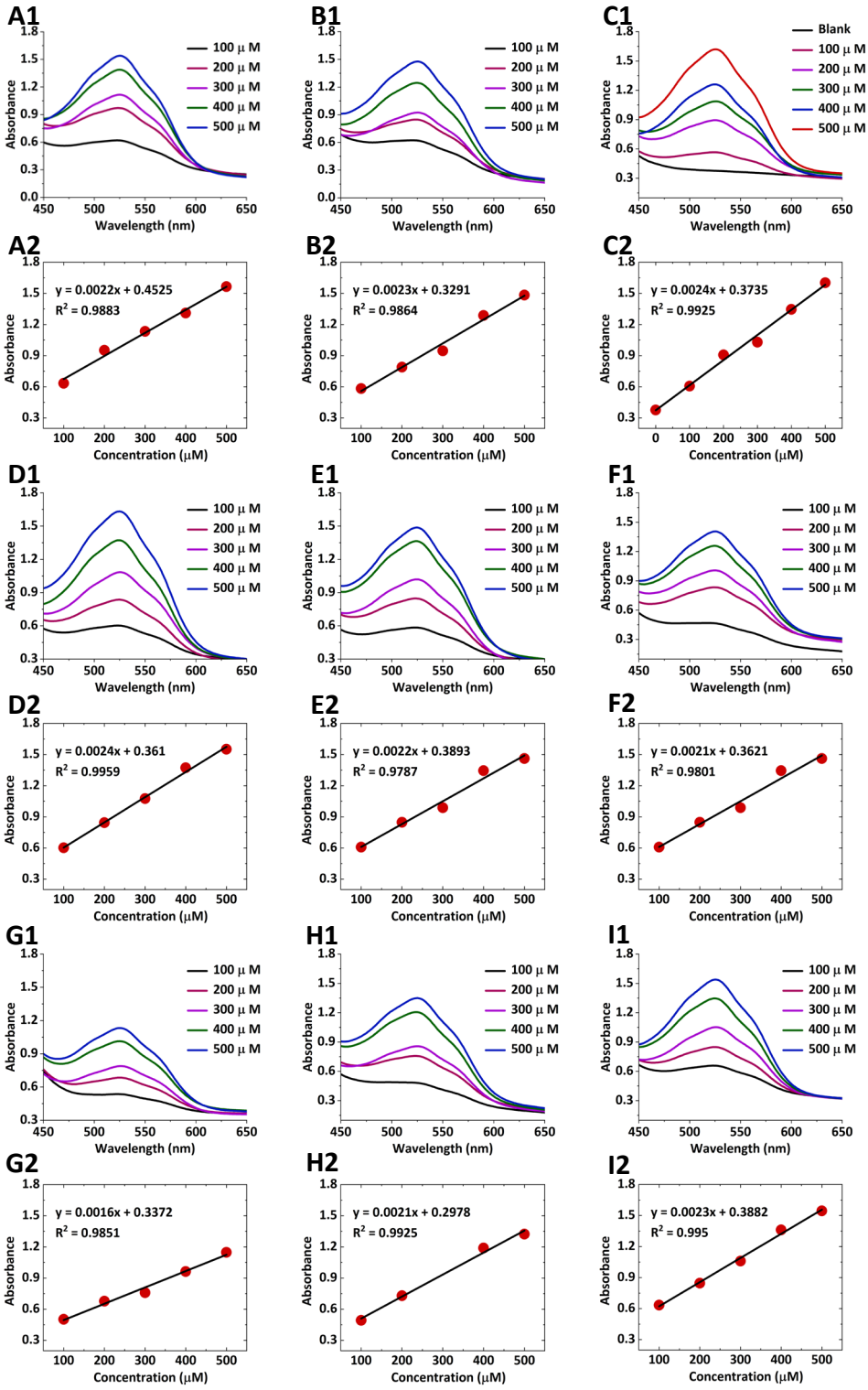

Figure S5: Urea calibration graphs Absorbance scans as a function of wavelengths. Absorbances as a function of urea concentrations at 525 nm. Different concentrations of urea were prepared in **A1, A2)** 1 M KNO_3 + 0.1 M $KHCO_3$ **B1, B2)** 0.5 M KNO_3 + 0.1 M $KHCO_3$ **C1, C2)** 0.1 M KNO_3 + 0.1 M $KHCO_3$ **D1, D2)** 0.01 M KNO_3 + 0.1 M $KHCO_3$ **E1, E2)** 0.001 M KNO_3 + 0.1 M $KHCO_3$ **F1, F2)** 0.1

M KNO_3 + 1 M $KHCO_3$ **G1, G2)** 0.1 M KNO_3 + 0.5 M $KHCO_3$ **H1, H2)** 0.1 M KNO_3 + 0.01 M $KHCO_3$ **I1, I2)** 0.1 M KNO_3 + 0.001 M $KHCO_3$.

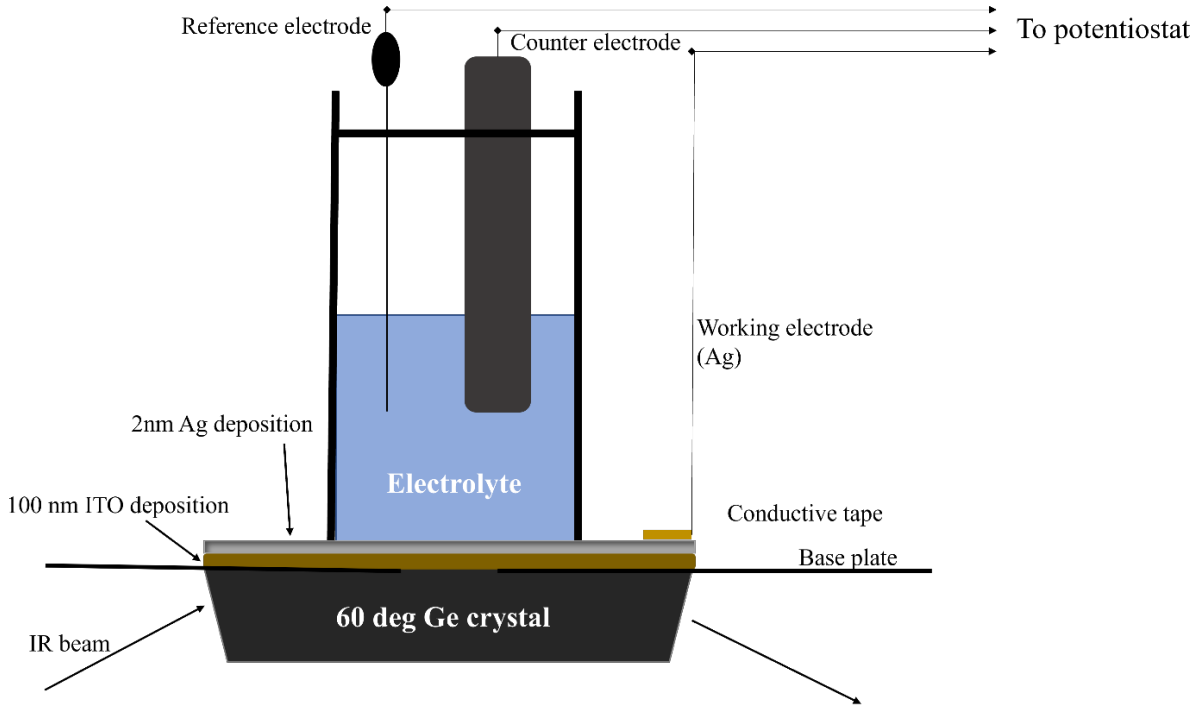

Figure S6: Schematic of the cell used for FTIR Studies

NH_3, urea, formamide, and methyl amine are the possible nitrogen-containing products. Figure S7 denotes the FTIR spectra of reactants and products. All these products have strong signature peaks between wavenumbers 2500 and 3500 cm^{-1}. The reactants $KHCO_3$ and KNO_3 do not have signatures in wavenumbers above 2000 cm^{-1}. Hence, we can use those regions to get insights from the in-situ FTIR data. Urea has a strong signature band between 3300 and 3500 cm^{-1}, corresponding to N-H stretching. NH_4Cl has the N-H stretching signature from 2800 to 3300 cm^{-1}. Hence, urea and NH_3 signatures can be easily distinguished from each other using the N-H stretching feature. Formamide has N-H stretching band in the same region as urea, and in addition, formamide has C-H stretching band between 2750 and 3000 cm^{-1}, which is absent in urea. Hence, urea and formamide could be distinguished using the C-H stretching band. Methyl amine has a strong C-H stretching band between 2750 and 3000 cm^{-1} but not a dominant N-H stretching band. Formamide and urea also have strong signatures corresponding to C=O stretching between 1500 and 1750 cm^{-1}. C=O stretching is absent in NH_3 and methyl amine. Methyl amine, urea, and formamide have C-N stretching features between 750 and 1500 cm^{-1}, missing in NH_3. Hence, we can use these features to distinguish the products and analyze the in-situ FTIR data.

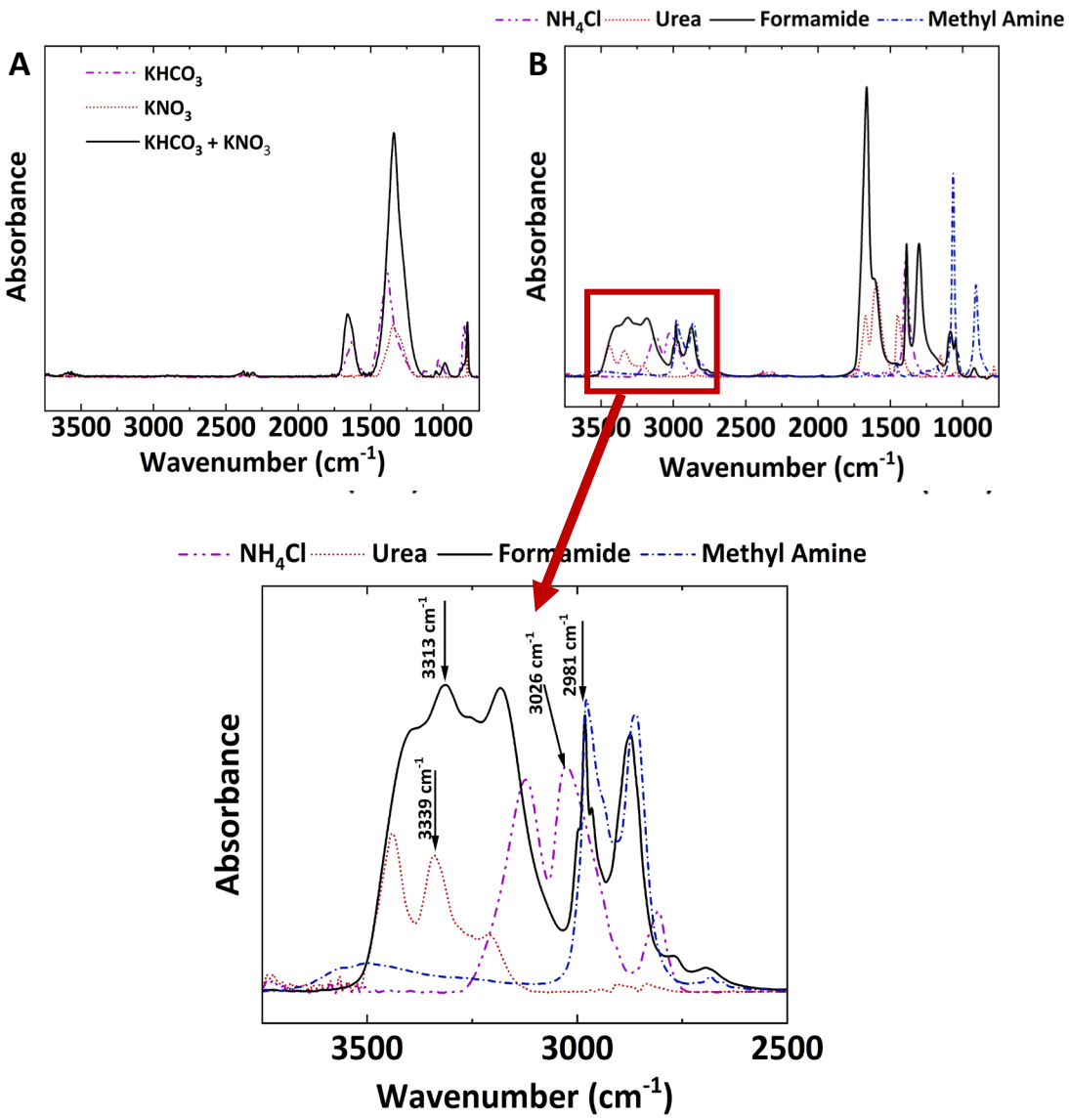

Figure S7: Fourier Transform Infrared (FTIR) Spectroscopy A) FTIR Spectra of reactants (CO_2 sparged $KHCO_3$ and KNO_3). B) FTIR Spectra of possible products.

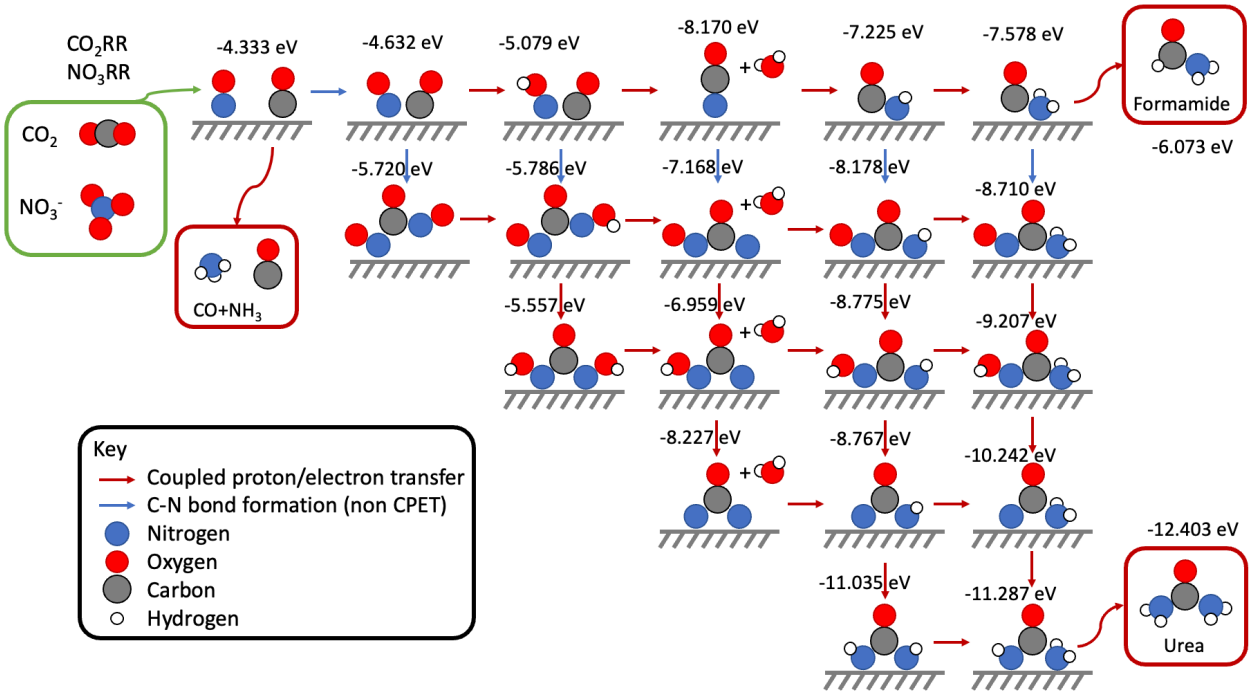

Figure S8: Possible pathways considered for the electrochemical urea synthesis from CO_2 and NO_3^-.

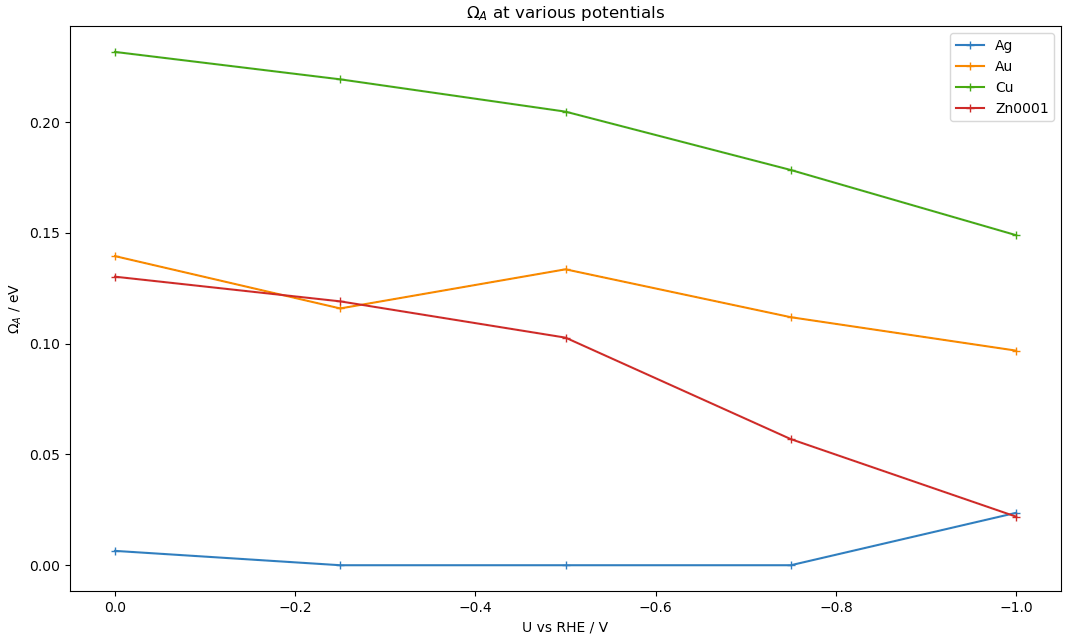

Figure S9: First C-N bond formation barrier on selected materials (*CO + *NO → *CONO)

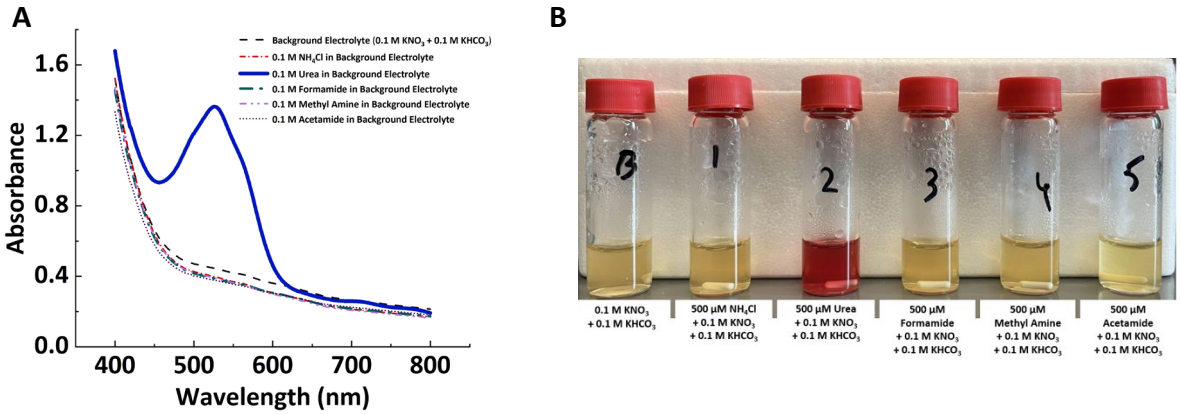

Figure S10: A) Absorbance as a function of wavelength for different possible products. B) Photograph of the color change when the reagents are added for the diacetylmonoxime method. Only urea shows the color change and other products donot show any change in color.

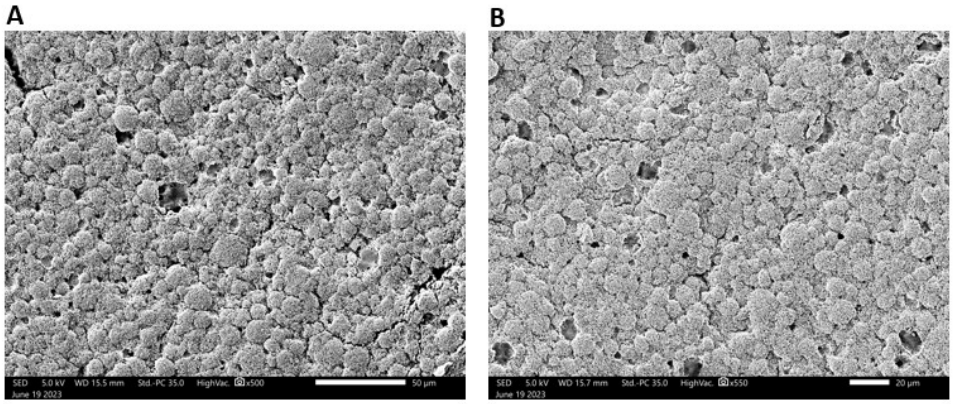

Figure S11: Scanning Electron Microscopy (SEM) A) SEM image of Ag GDE pre-electrolysis (50µm). B) SEM image of Ag GDE post-electrolysis (20 µm).

The co-adsorption free energy of CO_2 and NO3- :

The co-adsorption free energy of CO2 and NO3- will occur through two coupled proton-electron transfer step as shown in Eq S1. The co-adsorption free energy is calculated to be -0.83eV at 0 V vs. RHE

$$NO_3^-(aq) + CO_2(g) + 2H_2O + 2e^- + 2 * \rightarrow * NO_2 + * COOH + 3OH^- \quad (1)$$

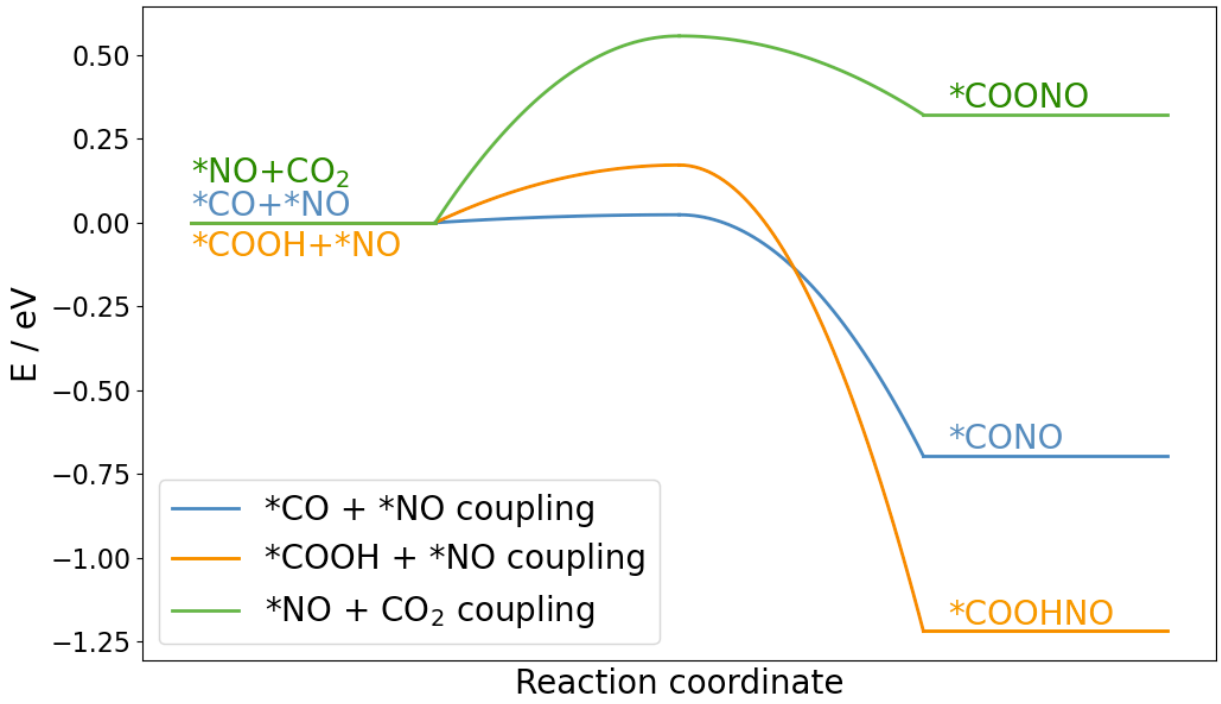

Figure S12: First C-N bond formation barrier on Ag(100)

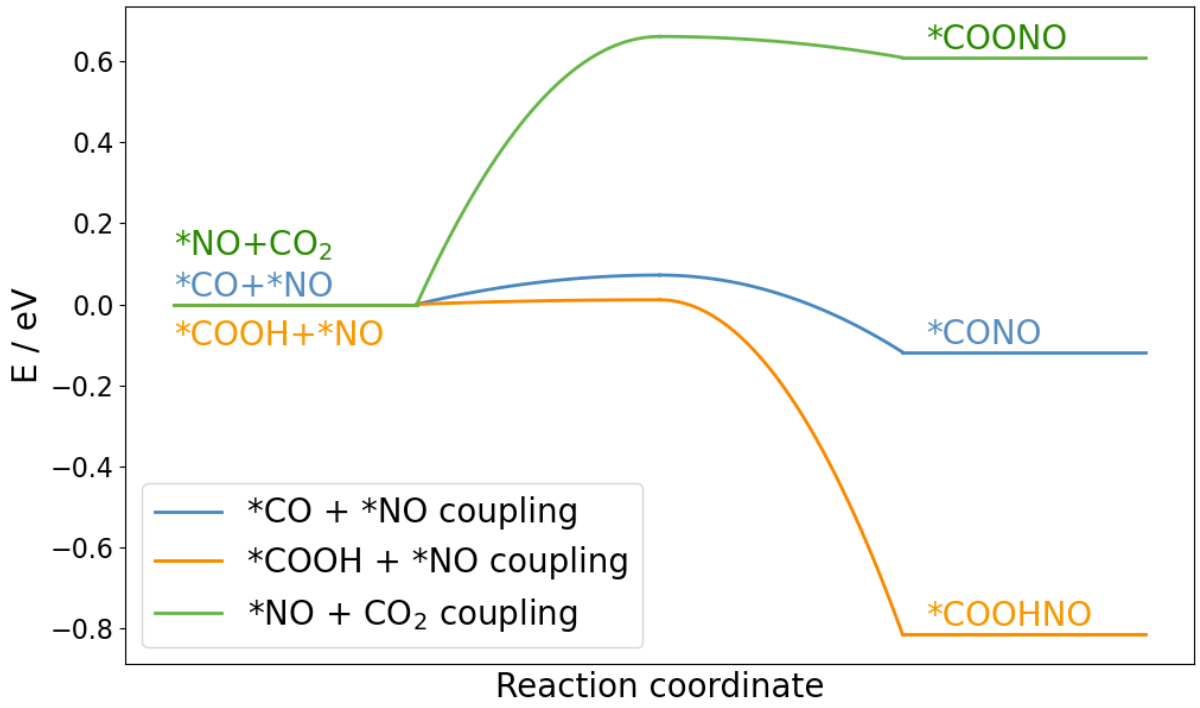

Figure S13: First C-N bond formation barrier on Ag(111)

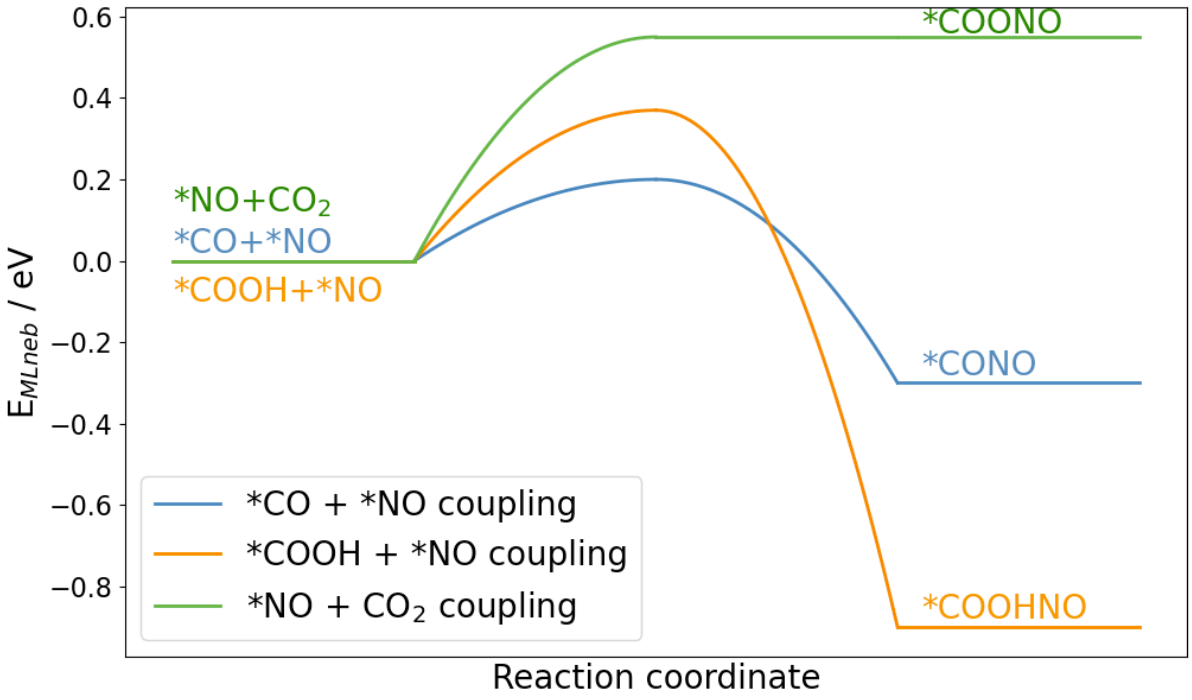

Figure S14: First C-N bond formation barrier on Ag(110)

The values of Coupling barriers on Figure S12 and Figure S13 were calculated using traditional DFT Nudge elastic Band (NEB) method. On Figure S14, the coupling barriers (E_{MLneb}) were estimated using Machine learning ML potentials from the Open catalyst Project (OCP) which has been known to be in good agreement with DFT values.[17, 18] This method was used due to the larger size of the Ag (110) system due to convergence and computational cost issues with the traditional DFT methods.

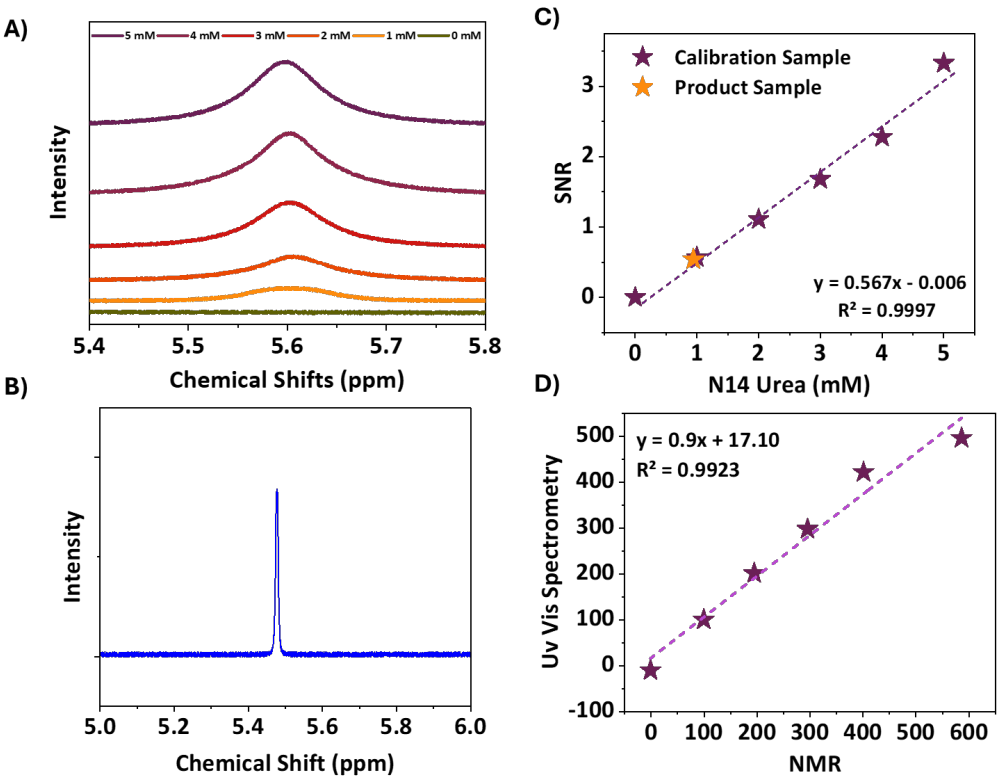

Figure S15: A) NMR spectra of urea calibration solutions B) Calibration plot for N14 Urea samples C)1-H NMR spectrum of post electrolysis sample showing a peak at a chemical shift of 5.5 ppm corresponding to urea and the FE is estimated to be ~98% D) Parity plot for NMR vs UV-vis spectrometry.

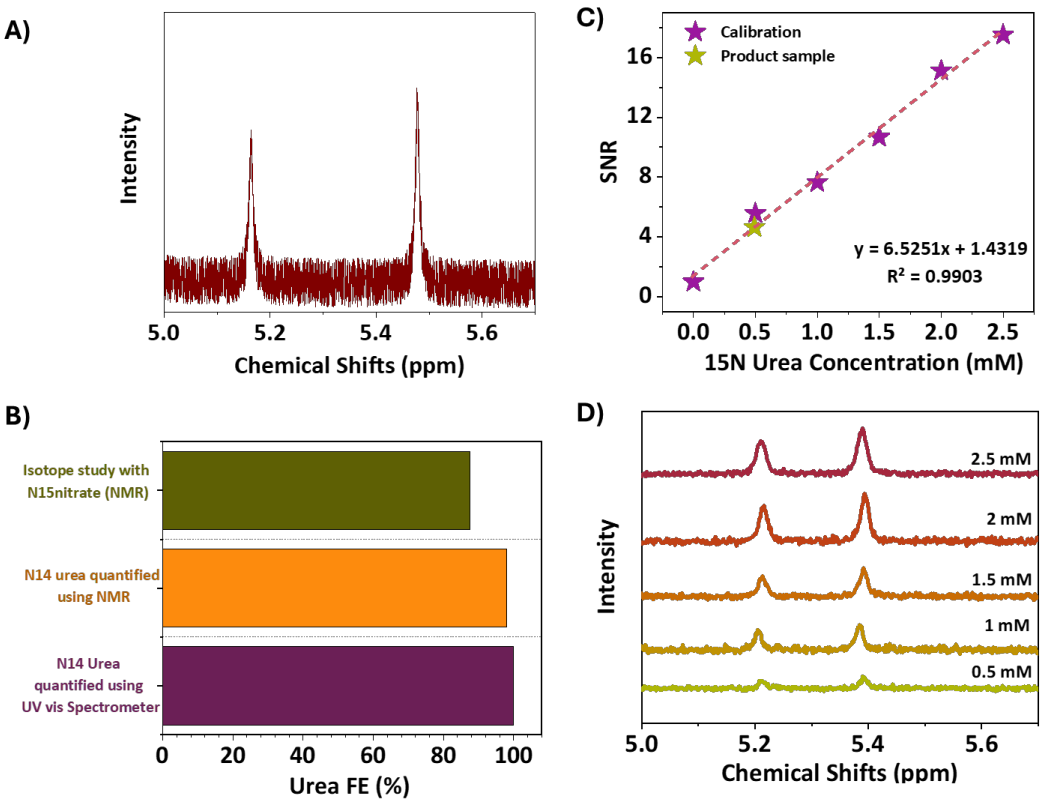

Figure S16: (A) ^{1}H NMR spectra of the post-electrolysis solution using $^{15}KNO_3$. The doublet observed indicates the presence of ^{15}N-labeled urea. (B) Calibration graph for ^{15}N-labeled urea solutions obtained using ^{1}H NMR. (C) Comparison of Faradaic efficiencies (FE) in the isotope-labeled study, with ^{14}N urea quantification performed using both ^{1}H NMR and UV-Vis spectrometry. (D) ^{1}H NMR spectra of the calibration solutions for ^{15}N-labeled urea.

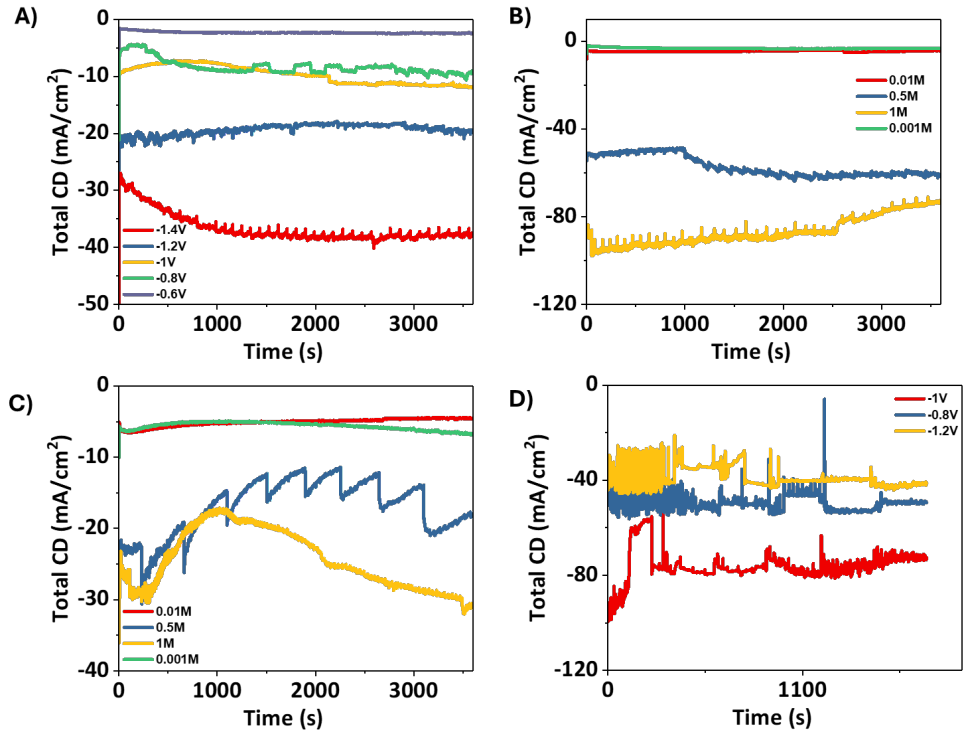

Figure S17: A) Current versus time data for the study on the effect of applied potential (all potentials referenced against RHE). B) Current versus time data showing the effect of varying KNO_3 concentration while keeping $KHCO_3$ constant at 0.1 M. C) Current versus time data illustrating the effect of varying $KHCO_3$ concentration while maintaining KNO_3 constant at 0.1 M. D) Current versus time data for the AgGDE (Ag Gas Diffusion Electrode) setup.

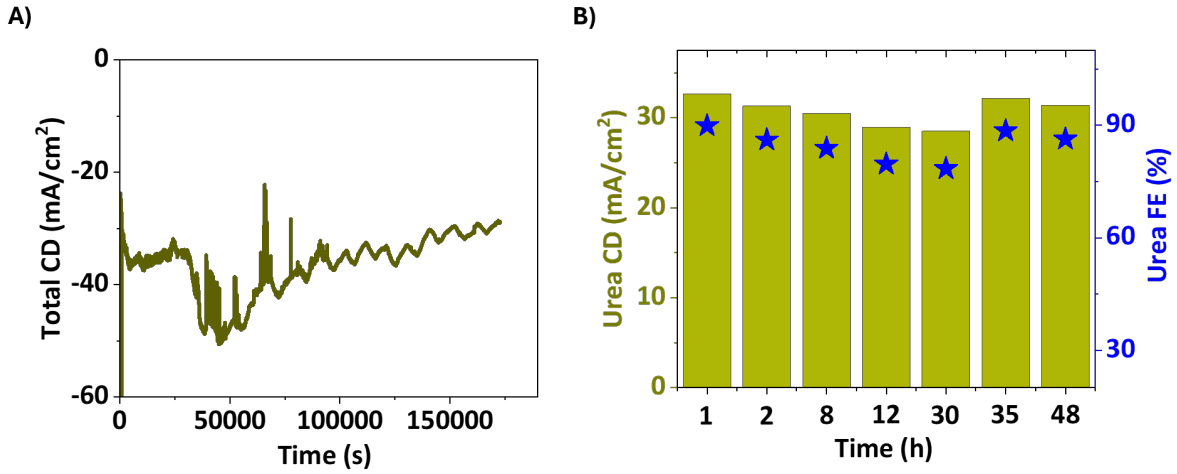

Figure S18: (A) Current versus time data demonstrating the 48-hour stability of the electrochemical setup. B) Faradaic efficiency (FE) for urea production and current densities (CDs) over time during the 48-hour stability test.

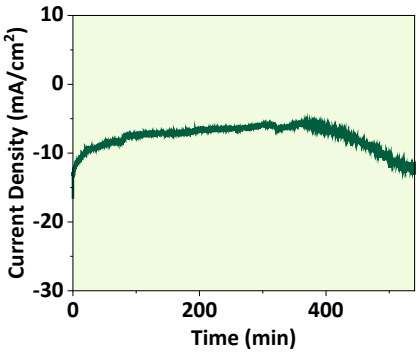

Figure S19: Current vs time data for 9 hour stability analysis

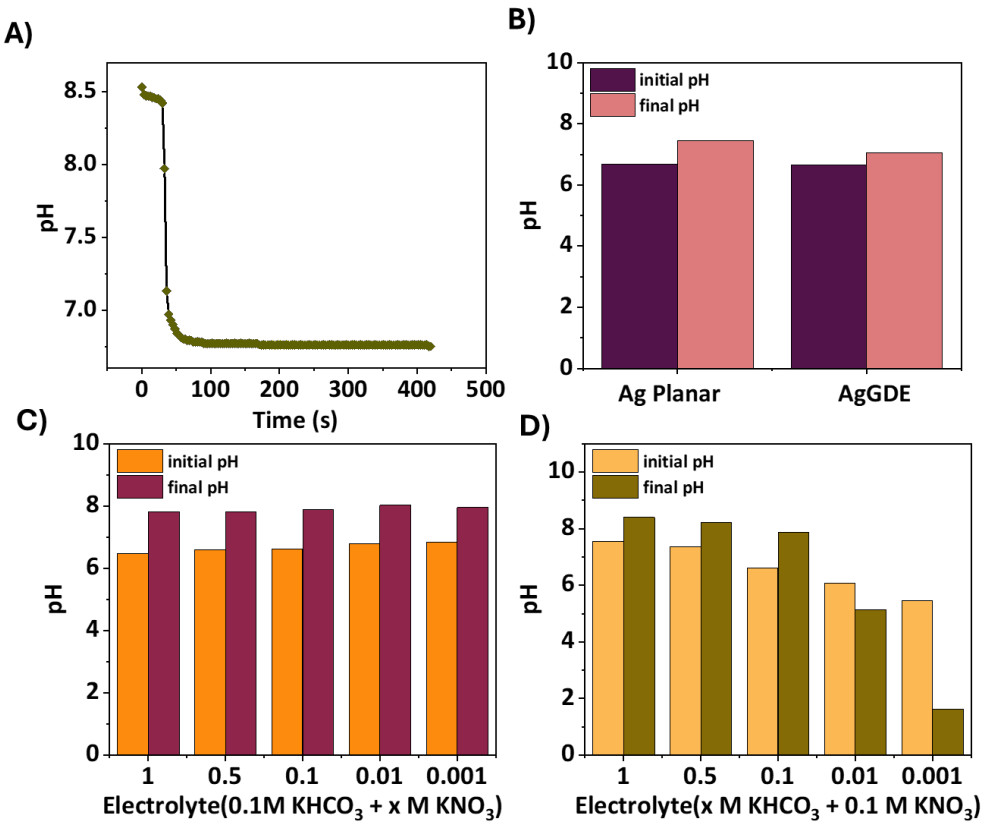

Figure S20: A) Change in pH with time while equilibrating electrolyte (0.1M KNO_3+ 0.1M $KHCO_3$) with gaseous CO_2. B) Initial pH and post reaction pH of electrolyte in Ag planar set up and Ag GDE set up. C) Initial pH and post reaction pH of electrolyte with varying KNO_3 concentration. D) Initial pH and post reaction pH of electrolyte with varying $KHCO_3$ concentration

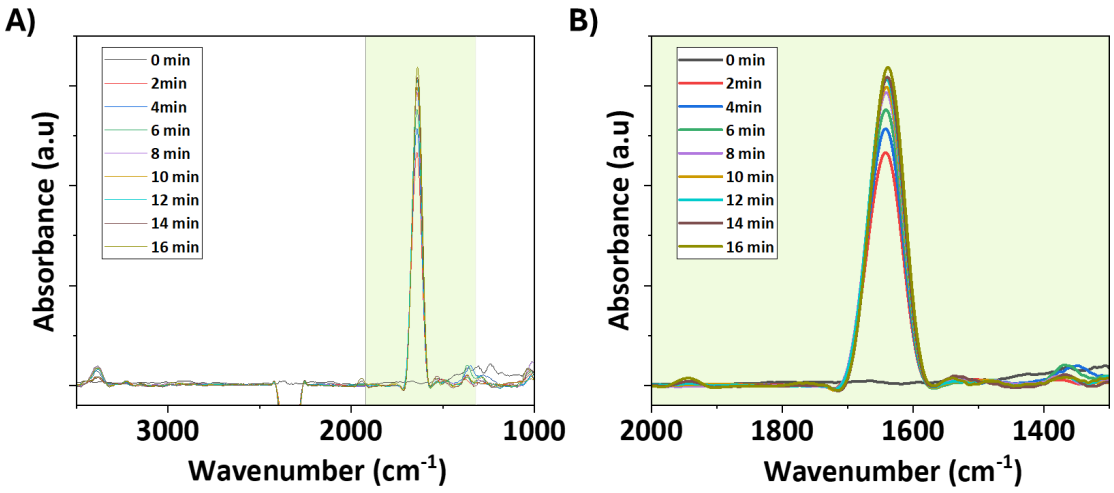

Figure S21: A) FTIR spectra showing stabilized state of CO intermediate B) Zoomed in version of spectra A)

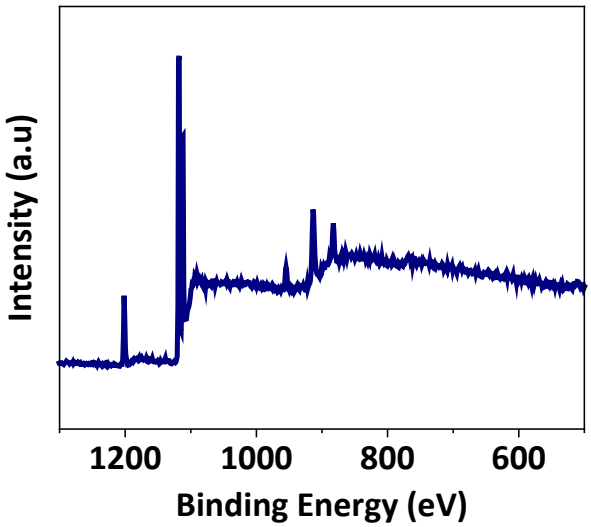

Figure S22: XPS survey scan for Ag planar electrode post electrolysis

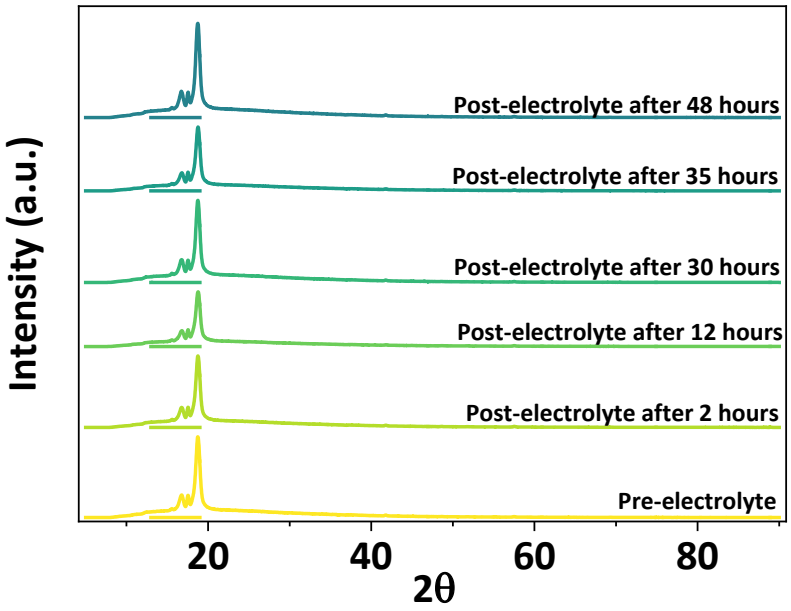

Figure S23: XRF analysis on post electrolysis samples during 48 hour stability test

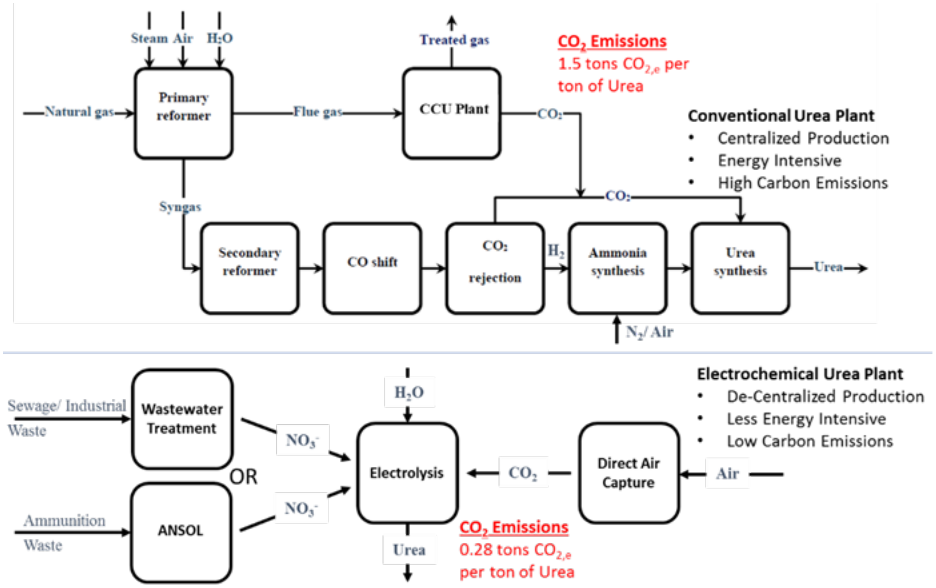

Figure S24: Block diagram of process flow for conventianal urea plant and the the proposed electrochemical urea plant that utilizes waste nitrates and CO_2.

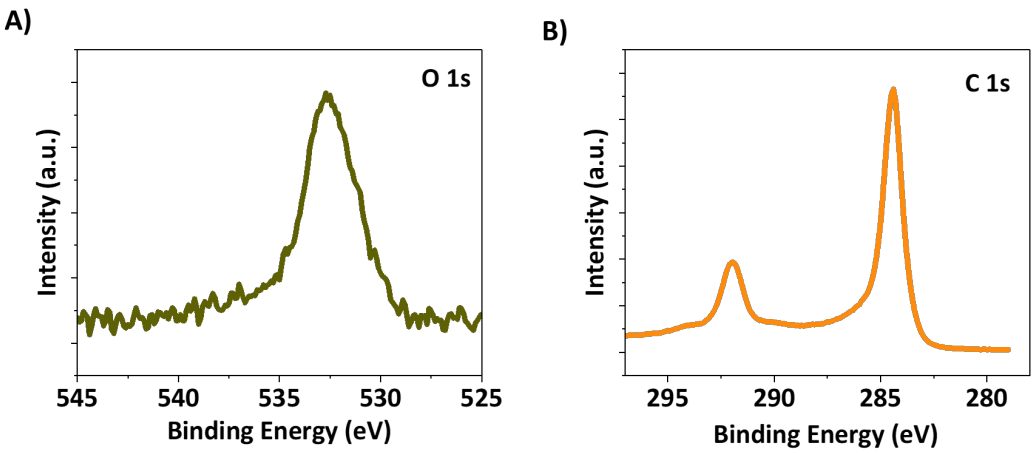

Figure S25: XPS of bare carbon substrate: A) O1s spectra B) C1s spectra

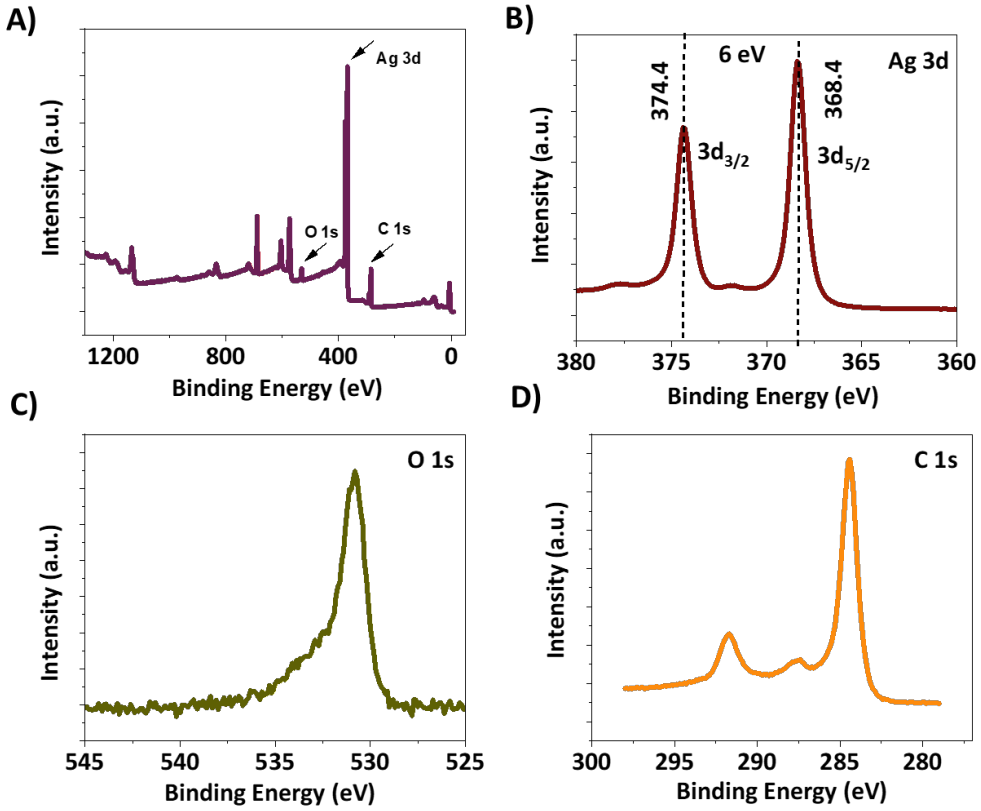

Figure S26: XPS of Pre electrolysis AgGDE: A) Survey Scan B) Ag 3d spectra C) O 1s spectra D) C 1s spectra

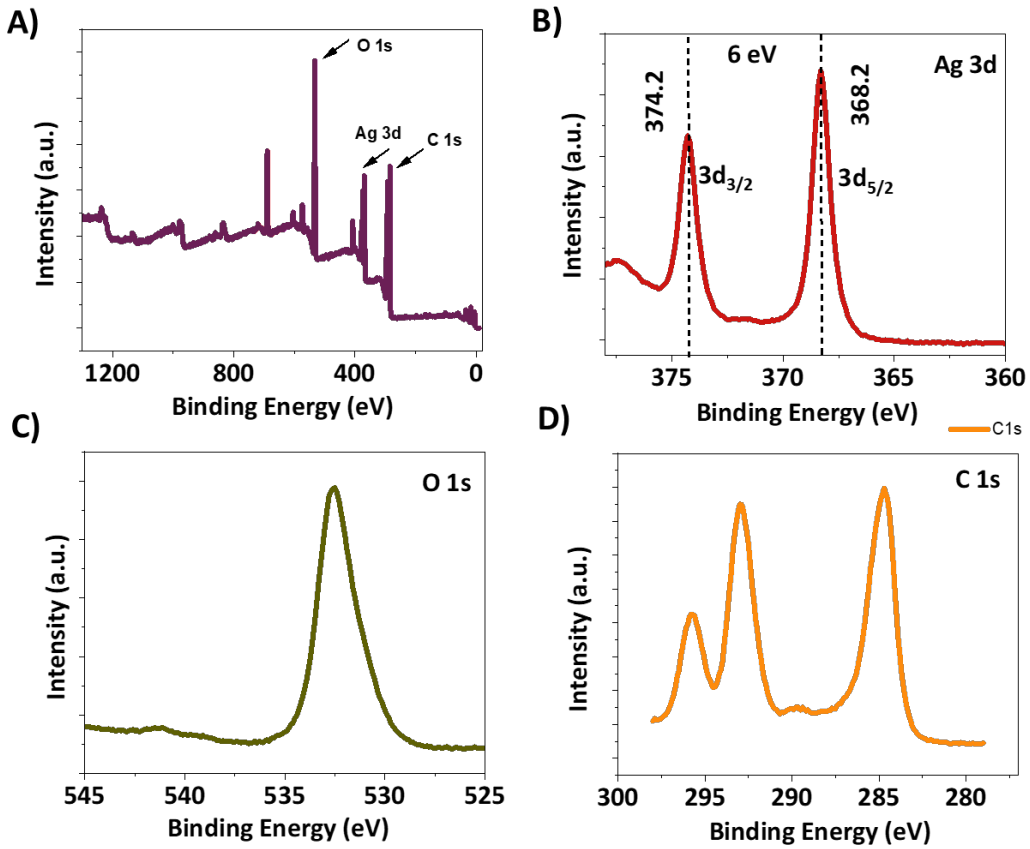

Figure S27: XPS of Post electrolysis AgGDE: A) Survey Scan B) Ag 3d spectra C) O 1s spectra D) C 1s spectra

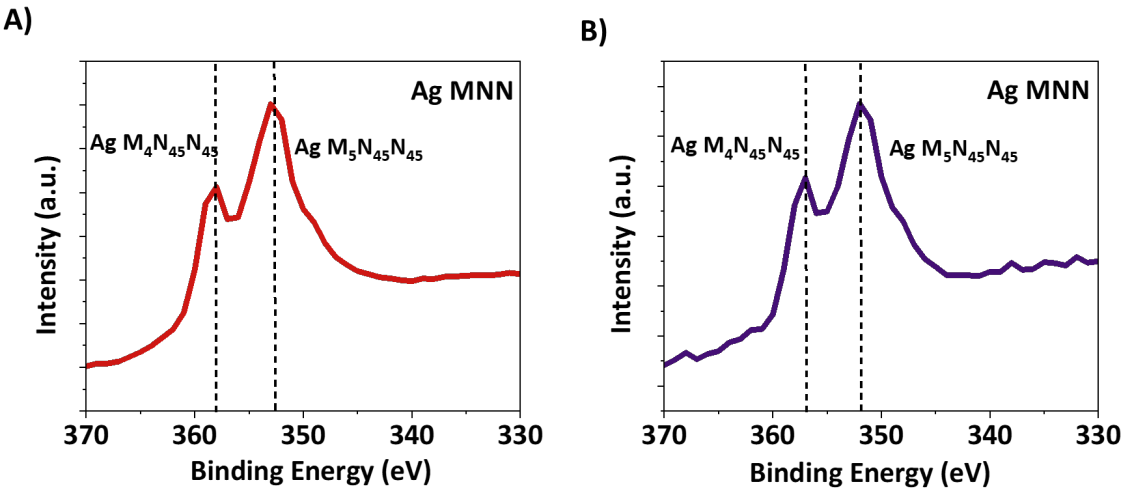

Figure S28: Auger Spectra: A) Ag MNN for pre-electrolysis AgGDE B) Ag MNN for post-electrolysis AgGDE

References

1. M. Yuan, J. Chen, Y. Bai, Z. Liu, J. Zhang, T. Zhao, Q. Shi, S. Li, X. Wang and G. Zhang, *Chemical Science*, 2021, **12**, 6048-6058.
2. M. Yuan, J. Chen, Y. Bai, Z. Liu, J. Zhang, T. Zhao, Q. Wang, S. Li, H. He and G. Zhang, *Angewandte Chemie*, 2021, **133**, 11005-11013.
3. Y. Feng, H. Yang, Y. Zhang, X. Huang, L. Li, T. Cheng and Q. Shao, *Nano Letters*, 2020, **20**, 8282-8289.
4. M. Shibata and N. Furuya, *Journal of Electroanalytical Chemistry*, 2001, **507**, 177-184.
5. J. Leverett, T. Tran-Phu, J. A. Yuwono, P. Kumar, C. Kim, Q. Zhai, C. Han, J. Qu, J. Cairney and A. N. Simonov, *Advanced Energy Materials*, 2022, **12**, 2201500.
6. M. Shibata, K. Yoshida and N. Furuya, *Journal of Electroanalytical Chemistry*, 1998, **442**, 67-72.
7. C. Lv, C. Lee, L. Zhong, H. Liu, J. Liu, L. Yang, C. Yan, W. Yu, H. H. Hng and Z. Qi, *ACS nano*, 2022.
8. C. Lv, L. Zhong, H. Liu, Z. Fang, C. Yan, M. Chen, Y. Kong, C. Lee, D. Liu and S. Li, *Nature Sustainability*, 2021, **4**, 868-876.
9. M. Shibata, K. Yoshida and N. Furuya, *Journal of the Electrochemical Society*, 1998, **145**, 2348.
10. N. Meng, Y. Huang, Y. Liu, Y. Yu and B. Zhang, *Cell Reports Physical Science*, 2021, **2**, 100378.
11. R. Shi and T. Zhang, *Science China Chemistry*, 2020, **63**, 1580-1581.
12. Y. Huang, R. Yang, C. Wang, N. Meng, Y. Shi, Y. Yu and B. Zhang, *ACS Energy Letters*, 2021, **7**, 284-291.
13. C. Chen, X. Zhu, X. Wen, Y. Zhou, L. Zhou, H. Li, L. Tao, Q. Li, S. Du and T. Liu, *Nature chemistry*, 2020, **12**, 717-724.
14. X. Zhang, X. Zhu, S. Bo, C. Chen, M. Qiu, X. Wei, N. He, C. Xie, W. Chen and J. Zheng, *Nature Communications*, 2022, **13**, 5337.
15. D. Saravanakumar, J. Song, S. Lee, N. H. Hur and W. Shin, *ChemSusChem*, 2017, **10**, 3999-4003.
16. J. Mukherjee, S. Paul, A. Adalder, S. Kapse, R. Thapa, S. Mandal, B. Ghorai, S. Sarkar and U. K. Ghorai, *Advanced Functional Materials*, 2022, **32**, 2200882.
17. R. Tran, J. Lan, M. Shuaibi, B. M. Wood, S. Goyal, A. Das, J. Heras-Domingo, A. Kolluru, A. Rizvi and N. Shoghi, *ACS Catalysis*, 2023, **13**, 3066-3084.
18. L. Chanussot, A. Das, S. Goyal, T. Lavril, M. Shuaibi, M. Riviere, K. Tran, J. Heras-Domingo, C. Ho and W. Hu, *Acs Catalysis*, 2021, **11**, 6059-6072.